J. Fluid Mech. (2019), *vol.* 861, *pp.* 163–179.
doi:10.1017/jfm.2018.924

On the Reynolds number dependence of velocity-gradient structure and dynamics

Rishita Das[1,†] **and Sharath S. Girimaji**[1,2]

[1]Department of Aerospace Engineering, Texas A&M University, College Station, TX 77843, USA

[2]Department of Ocean Engineering, Texas A&M University, College Station, TX 77843, USA

(Received 30 May 2018; revised 21 September 2018; accepted 8 November 2018;
first published online 19 December 2018)

We seek to examine the changes in velocity-gradient structure (local streamline topology) and related dynamics as a function of Reynolds number (Re_λ). The analysis factorizes the velocity gradient (A_{ij}) into the magnitude (A^2) and normalized-gradient tensor ($b_{ij} \equiv A_{ij}/\sqrt{A^2}$). The focus is on bounded b_{ij} as (i) it describes small-scale structure and local streamline topology, and (ii) its dynamics is shown to determine magnitude evolution. Using direct numerical simulation (DNS) data, the moments and probability distributions of b_{ij} and its scalar invariants are shown to attain Re_λ independence. The critical values beyond which each feature attains Re_λ independence are established. We proceed to characterize the Re_λ dependence of b_{ij}-conditioned statistics of key non-local pressure and viscous processes. Overall, the analysis provides further insight into velocity-gradient dynamics and offers an alternative framework for investigating intermittency, multifractal behaviour and for developing closure models.

Key words: intermittency, isotropic turbulence, turbulent flows

1. Introduction

Velocity-gradient dynamics underlies many critical turbulence phenomena such as intermittency, multifractality, streamline topology, material-element deformation and scalar mixing (Soria *et al.* 1994; Blackburn, Mansour & Cantwell 1996; Martín *et al.* 1998*b*; Suman & Girimaji 2010; Danish, Suman & Girimaji 2016). It is of fundamental interest to understand velocity-gradient dynamics and develop Lagrangian closure models that capture key turbulence features (Girimaji & Pope 1990; Martín, Dopazo & Valiño 1998*a*; Jeong & Girimaji 2003; Chevillard *et al.* 2008; Meneveau 2011; Pereira, Moriconi & Chevillard 2018). The multifractal and intermittent nature of velocity gradients renders characterization of their dynamics quite challenging (Yakhot & Sreenivasan 2005; Donzis, Yeung & Sreenivasan 2008; Yeung, Zhai & Sreenivasan 2015). It has been demonstrated in recent literature (Yakhot & Donzis 2017) that intermittency effects manifest even at Reynolds number $Re_\lambda \sim O(10)$ and are significant by $Re_\lambda \sim O(100)$. To complement the findings of the above studies, the goal of this investigation is to establish the Re_λ dependence of the internal structure of the velocity gradients and constituent dynamical processes. We demonstrate that such

†Email address for correspondence: rishitadas@tamu.edu

an examination leads to improved insight into important aspects of velocity-gradient dynamics, including a clear distinction between internal structure and magnitude effects.

We factorize the velocity-gradient tensor (A_{ij}) into the magnitude (A^2-Frobenius norm of $\boldsymbol{A}$) and normalized velocity-gradient tensor $\boldsymbol{b}$ (Girimaji & Speziale 1995; Bikkani & Girimaji 2007; Bechlars & Sandberg 2017):

$$b_{ij} = \frac{A_{ij}}{A} \quad \text{where } A = \sqrt{A^2} = \sqrt{A_{mn}A_{mn}}. \tag{1.1}$$

The tensor $\boldsymbol{b}$ is of intrinsic physical interest as it provides insight into many structural features of turbulence such as local streamline topology and the orientation between strain rate eigendirections and vorticity (Ashurst *et al.* 1987; Wang *et al.* 2014). The tensor b_{ij} is mathematically bounded and thus expected to be more amenable to analysis and closure modelling. Furthermore, it is demonstrated that the processes requiring closure in the equations for b_{ij} and A^2 are identical. Thus, the evolution of unbounded-A^2 can be cast in terms of bounded-b_{ij} dynamics.

The goal of the present study is to exploit the bounded nature of the b_{ij} tensor to examine the velocity-gradient structure and non-local processes. We seek to:

(i) Develop appropriately scaled b_{ij} and A^2 evolution equations and exhibit that the processes requiring closure in the two cases are similar.

(ii) Examine the Re_λ dependence of the velocity-gradient structure: b_{ij}-moments, probability density functions (PDFs) and invariants (q and r). Although q and r are bounded, the normalization does not guarantee self-similarity at different Reynolds numbers.

(iii) Establish the Re_λ dependence of the unclosed non-local pressure and viscous processes in the b_{ij} and A^2 evolution equations conditioned upon q and r.

The work employs forced isotropic turbulence simulation data in the Taylor-scale Reynolds number range $Re_\lambda = 1$ to 588. The remainder of the paper is arranged as follows. Section 2 contains the evolution equations of A^2, b_{ij} and its invariants. A brief description of the data sets used in the study is given in § 3. The Re_λ dependences of various velocity-gradient features are presented in § 4. The paper concludes in § 5 with a brief summary.

2. Governing equations

Differentiating the incompressible Navier Stokes equation with respect to spatial coordinates (x_j) yields the evolution equation of the velocity-gradient tensor (Cantwell 1992),

$$\frac{\mathrm{d}}{\mathrm{d}t}(A_{ij}) + A_{ik}A_{kj} = -\frac{\partial^2 p}{\partial x_i \partial x_j} + \nu \frac{\partial^2 A_{ij}}{\partial x_k \partial x_k}; \quad i, j = 1, 2, 3. \tag{2.1}$$

Using the incompressibility condition $A_{ii} = 0$, the isotropic pressure Hessian term can be written as

$$A_{ik}A_{ki} = -\frac{\partial^2 p}{\partial x_i \partial x_i}. \tag{2.2}$$

The non-local anisotropic pressure Hessian and the viscous diffusion term are

$$H_{ij} = -\frac{\partial^2 p}{\partial x_i \partial x_j} + \frac{\partial^2 p}{\partial x_k \partial x_k}\frac{\delta_{ij}}{3}; \quad T_{ij} = \nu \frac{\partial^2 A_{ij}}{\partial x_k \partial x_k}. \tag{2.3a,b}$$

Thus, the velocity-gradient equation may be written as

$$\frac{\mathrm{d}A_{ij}}{\mathrm{d}t} + A_{ik}A_{kj} - \frac{1}{3}A_{mk}A_{km}\delta_{ij} = H_{ij} + T_{ij}. \tag{2.4}$$

In a Lagrangian reference frame, the A_{ij}-dynamics depends upon the non-local pressure and viscous terms. One of the earliest attempts at developing closure models for velocity-gradient dynamics was made by Vieillefosse (1982) by neglecting the non-local terms. There have since been several Lagrangian velocity-gradient models that develop closure for H_{ij} and T_{ij} to replicate turbulence behaviour. However, the intermittent nature of the velocity-gradient magnitude renders the modelling rather challenging. Recently, Pereira *et al.* (2018) have used multifractal considerations, to first model A^2 and then determine the closure for A_{ij}-evolution.

We seek an alternative approach by segregating the evolution of the magnitude (A^2) from that of normalized velocity-gradient tensor b_{ij} as defined in (1.1). We propose that modelling b_{ij} first has advantages due to the boundedness of the tensor components. Further, b_{ij} is of intrinsic interest as it characterizes the orientation of velocity gradients and local flow structures.

2.1. *Mathematical bounds of* b_{ij}

Longitudinal b_{ij}-components satisfy the incompressibility condition,

$$b_{ii} = b_{11} + b_{22} + b_{33} = 0, \tag{2.5}$$

$$\Rightarrow b_{33} = -(b_{11} + b_{22}). \tag{2.6}$$

By virtue of normalization, the following inequality holds true:

$$b_{11}^2 + b_{22}^2 + b_{33}^2 \leqslant 1. \tag{2.7}$$

Applying (2.6) in the above inequality we obtain the following constraint:

$$b_{11}^2 + b_{22}^2 + b_{11}b_{22} \leqslant \tfrac{1}{2}. \tag{2.8}$$

The bounds of b_{11} subject to the above constraint can be obtained as

$$\tfrac{1}{2}\left(-\sqrt{2 - 3b_{22}^2} - b_{22}\right) \leqslant b_{11} \leqslant \tfrac{1}{2}\left(\sqrt{2 - 3b_{22}^2} - b_{22}\right). \tag{2.9}$$

Now let us examine the minimum possible value of the lower bound. Minimizing the lower bound yields a b_{22} value of

$$b_{22} = \tfrac{1}{\sqrt{6}}. \tag{2.10}$$

Similarly, the upper bound attains the maximum value when

$$b_{22} = -\tfrac{1}{\sqrt{6}}. \tag{2.11}$$

Therefore, b_{11} or any other longitudinal velocity gradient is bounded as

$$-\sqrt{\tfrac{2}{3}} \leqslant b_{ij} \leqslant \sqrt{\tfrac{2}{3}} \quad \forall i = j. \tag{2.12}$$

Transverse components can be the sole non-zero element in the velocity-gradient tensor. These components are only constrained by normalization and are therefore only limited by unity,

$$-1 \leqslant b_{ij} \leqslant 1 \quad \forall i \neq j. \tag{2.13}$$

2.2. *Evolution equations of A^2 and b_{ij}*

Multiplying the velocity-gradient equation (2.4) through by A_{ij}/A^3 yields

$$\frac{A_{ij}}{A^3}\frac{\mathrm{d}}{\mathrm{d}t}(A_{ij}) = -\frac{A_{ij}A_{ik}A_{kj}}{A^3} + \frac{1}{3A^3}A_{km}A_{mk}\delta_{ij}A_{ij} + \frac{A_{ij}H_{ij}}{A^3} + \frac{A_{ij}T_{ij}}{A^3}. \tag{2.14}$$

Using the incompressibility condition, we obtain the following equation:

$$\frac{1}{A^3}\frac{\mathrm{d}A^2}{\mathrm{d}t} = \frac{1}{A^3}\frac{\mathrm{d}}{\mathrm{d}t}(A_{ij}A_{ij}) = -2b_{ij}b_{ik}b_{kj} + 2b_{ij}h_{ij} + 2b_{ij}\tau_{ij}, \tag{2.15}$$

where the non-local physics is incumbent in the normalized anisotropic pressure Hessian and viscous diffusion terms:

$$h_{ij} = \frac{H_{ij}}{A^2} \quad \text{and} \quad \tau_{ij} = \frac{T_{ij}}{A^2}. \tag{2.16a,b}$$

It is convenient to describe magnitude evolution in terms of $\theta \equiv \log(A^2)$:

$$\frac{\mathrm{d}\theta}{\mathrm{d}t'} = I_\theta + \mathcal{P}_\theta + V_\theta; \tag{2.17}$$

where the normalized time and inertial, pressure and viscous contributions are

$$t' \triangleq At, \quad I_\theta = -2b_{ij}b_{ik}b_{kj}, \quad \mathcal{P}_\theta = 2b_{ij}h_{ij}, \quad V_\theta = 2b_{ij}\tau_{ij}. \tag{2.18a–d}$$

Next we turn our attention to the evolution of the normalized tensor b_{ij}:

$$\frac{\mathrm{d}b_{ij}}{\mathrm{d}t} = \frac{\mathrm{d}}{\mathrm{d}t}\left(\frac{A_{ij}}{A}\right) = \frac{1}{A}\frac{\mathrm{d}A_{ij}}{\mathrm{d}t} - \frac{A_{ij}}{2}\left(\frac{1}{A^3}\frac{\mathrm{d}A^2}{\mathrm{d}t}\right). \tag{2.19}$$

Using (2.4), (2.15) and (2.19), the governing equation for b_{ij} is obtained in normalized time t':

$$\frac{\mathrm{d}b_{ij}}{\mathrm{d}t'} = -b_{ik}b_{kj} + h_{ij} + \tau_{ij} + \frac{1}{3}b_{mk}b_{km}\delta_{ij} + b_{ij}(b_{mk}b_{kn} - h_{mn} - \tau_{mn})b_{mn}. \tag{2.20}$$

The processes that require closure in the b_{ij}-equation – the non-local pressure term h_{ij} and viscous term τ_{ij} – are same as those in the A^2-equation. Although the boundedness of h_{ij} and τ_{ij} are not guaranteed, the requirement that b_{ij} be bounded renders modelling the pressure and viscous terms more tractable. Once the b_{ij}-evolution closure model equation is developed, the magnitude equation requires no further closure modelling.

2.3. *Evolution of b_{ij} invariants*

Let p, q and r represent the invariants of $\boldsymbol{b}$:

$$p = -b_{ii} = 0, \quad q = -\tfrac{1}{2}b_{im}b_{mi}, \quad r = -\tfrac{1}{3}b_{im}b_{mk}b_{ki}. \tag{2.21a–c}$$

These invariants are of interest as the local streamline structure can be classified into four distinct topologies based on q and r (Chong, Perry & Cantwell 1990). Now, we seek equations for q and r. Using (2.20), the following equation for inner product of $\boldsymbol{b}$ is obtained

$$\begin{aligned}\frac{\mathrm{d}}{\mathrm{d}t'}(b_{in}b_{nj}) \;=\; & -2b_{ik}b_{kn}b_{nj} + \frac{2}{3}b_{mk}b_{km}b_{ij} + 2b_{in}b_{nj}b_{mq}b_{mk}b_{kq} + h_{in}b_{nj} + b_{in}h_{nj} \\ & - 2h_{mq}b_{mq}b_{in}b_{nj} + \tau_{in}b_{nj} + b_{in}\tau_{nj} - 2\tau_{mq}b_{mq}b_{in}b_{nj}.\end{aligned} \tag{2.22}$$

Taking the trace of (2.22), the evolution equation of q is determined as

$$\frac{\mathrm{d}q}{\mathrm{d}t'} = -3r + 2qb_{ij}b_{ik}b_{kj} - h_{in}(b_{ni} + 2qb_{in}) - \tau_{in}(b_{ni} + 2qb_{in}) = I_q + \mathcal{P}_q + V_q, \quad (2.23)$$

where I_q, $\mathcal{P}_q$ and V_q represent inertial, pressure and viscous contributions towards the evolution of q:

$$I_q = -3r + 2qb_{ij}b_{ik}b_{kj}, \quad \mathcal{P}_q = -h_{in}(b_{ni} + 2qb_{in}), \quad V_q = -\tau_{in}(b_{ni} + 2qb_{in}). \quad (2.24a\text{–}c)$$

To obtain the equation of r, we first derive the equation for triple inner product of $\boldsymbol{b}$ using (2.20) and (2.22):

$$\begin{aligned}\frac{\mathrm{d}}{\mathrm{d}t'}(b_{il}b_{ln}b_{nj}) \;=\; & -3b_{il}b_{lk}b_{kn}b_{nj} + b_{il}b_{lj}b_{mk}b_{km} + 3b_{il}b_{ln}b_{nj}b_{mq}b_{mk}b_{kq} + (b_{il}h_{ln}b_{nj} \\ & + b_{il}b_{ln}h_{nj} + h_{il}b_{ln}b_{nj} - 3h_{mq}b_{mq}b_{il}b_{ln}b_{nj}) + (b_{il}\tau_{ln}b_{nj} + b_{il}b_{ln}\tau_{nj} \\ & + \tau_{il}b_{ln}b_{nj} - 3\tau_{mq}b_{mq}b_{il}b_{ln}b_{nj})\,. \end{aligned} \quad (2.25)$$

Applying the Cayley–Hamilton Theorem,

$$b_{il}b_{lk}b_{kj} + pb_{ik}b_{kj} + qb_{ij} + r\delta_{ij} = 0, \quad (2.26)$$

in the trace of (2.25), the evolution equation of r is obtained as follows:

$$\frac{\mathrm{d}r}{\mathrm{d}t'} = \frac{2}{3}q^2 + 3rb_{ij}b_{ik}b_{kj} - h_{mn}(b_{im}b_{ni} + 3rb_{mn}) - \tau_{mn}(b_{im}b_{ni} + 3rb_{mn}) = I_r + \mathcal{P}_r + V_r, \quad (2.27)$$

where the local (inertial and isotropic pressure), anisotropic pressure and viscous contributions in the evolution of r are

$$I_r = \tfrac{2}{3}q^2 + 3rb_{ij}b_{ik}b_{kj}, \quad \mathcal{P}_r = -h_{mn}(b_{im}b_{ni} + 3rb_{mn}), \quad V_r = -\tau_{mn}(b_{im}b_{ni} + 3rb_{mn}). \quad (2.28a\text{–}c)$$

The goal of the remainder of this paper is to use DNS data sets to establish the Re_λ dependence of the statistics of b_{ij}, q and r. Then we will also characterize the effect of changing Reynolds number on unclosed pressure (h_{ij}) and viscous (τ_{ij}) processes by examining the evolution of q, r and θ. The investigation of the unclosed invariants will yield further insight into velocity-gradient dynamics and provide guidance for developing closure models.

3. DNS data sets

DNS data sets used in this study have been obtained from the following sources: Donzis research group at Texas A&M University (Donzis *et al.* 2008; Yakhot & Donzis 2017) and Johns Hopkins Turbulence Database (Li *et al.* 2008). These data sets have been widely used in the literature to study velocity-gradient dynamics, intermittency and anomalous scaling (Donzis *et al.* 2008; Donzis & Sreenivasan 2010; Johnson & Meneveau 2016; Yakhot & Donzis 2017). Twelve forced isotropic incompressible turbulence data sets with Taylor Reynolds number (Re_λ) ranging from 1 to 588 are used in this work. The details of these simulations are shown in table 1. Here,

$$Re_\lambda \equiv u'\lambda/\nu \quad (3.1)$$

Re_λ	Grid points	$k_{max}\eta$	Source
1	256^3	105.6	Yakhot & Donzis (2017)
6	256^3	34.8	Yakhot & Donzis (2017)
9	256^3	26.6	Yakhot & Donzis (2017)
14	256^3	19.87	Yakhot & Donzis (2017)
18	256^3	15.59	Yakhot & Donzis (2017)
25	256^3	11.51	Yakhot & Donzis (2017)
35	64^3	1.45	Yakhot & Donzis (2017)
86	256^3	2.83	Donzis *et al.* (2008)
225	512^3	1.34	Donzis *et al.* (2008)
385	1024^3	1.41	Donzis *et al.* (2008)
414	1024^3	1.32	JHTDB: Li *et al.* (2008)
588	2048^3	1.39	Donzis *et al.* (2008)

TABLE 1. Details of forced isotropic incompressible turbulence data sets used.

where u' is the root-mean-square (r.m.s.) velocity and ν is the kinematic viscosity. λ (Taylor microscale) and ϵ (dissipation rate) are given by

$$\lambda = (15\nu(u')^2/\epsilon)^{1/2}, \quad \epsilon = 2\nu\langle S_{ij}S_{ij}\rangle. \tag{3.2a,b}$$

Here, $k_{max}\eta$ is the highest resolved wavenumber (k_{max}) normalized by the Kolmogorov length scale (η). All the derivatives used in this study are calculated using spectral methods.

4. Results and discussion

We start by exhibiting the known features of velocity gradients as a function of Reynolds number – anomalous scaling of the normalized higher-order moments and increasingly stretched exponential tails of the probability density functions (PDFs). We then contrast the known A_{ij} behaviour against the b_{ij} moments and PDF. Then the Re_λ dependence of various velocity-gradient dynamics processes conditioned on q and r is established.

4.1. *Unnormalized velocity-gradient statistics*

Even-order moments (M^A_{2n} for $n = 2, 3, 4, 5, 6$) of the longitudinal velocity gradient ($A_{11} = \partial u/\partial x$) given by

$$M^A_{2n} = \frac{\overline{{A_{11}}^{2n}}}{\overline{{A_{11}}^{2}}^{n}} \tag{4.1}$$

are plotted as a function of Re_λ in figure 1. Here, $\overline{(\,)}$ implies volume averaging. It is observed that for $Re_\lambda \leqslant 9$, the moments are nearly Gaussian. For $Re_\lambda > 9$, the values of all the moments steadily increase with Re_λ in agreement with the anomalous scaling observed by Yakhot & Donzis (2017). Note that the Re_λ-range considered in this study is much wider than that of Yakhot & Donzis (2017). Anomalous scaling of the moments is a clear indication of the intermittent behaviour of A_{ij}. This observation is further reinforced in the PDF plots of velocity gradients.

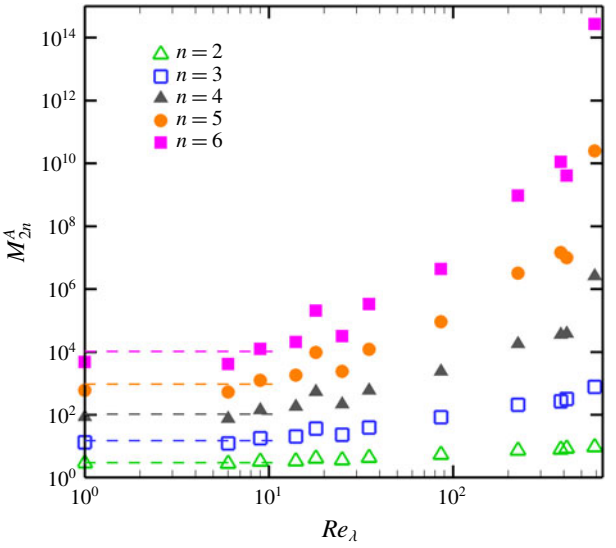

FIGURE 1. (Colour online) Even-order moments (M_{2n} for $n = 2, 3, 4, 5, 6$) of A_{11} as a function of Re_λ. Dashed lines represent Gaussian moments, i.e. $M^G_{2n} = (2n-1)!!$, for reference.

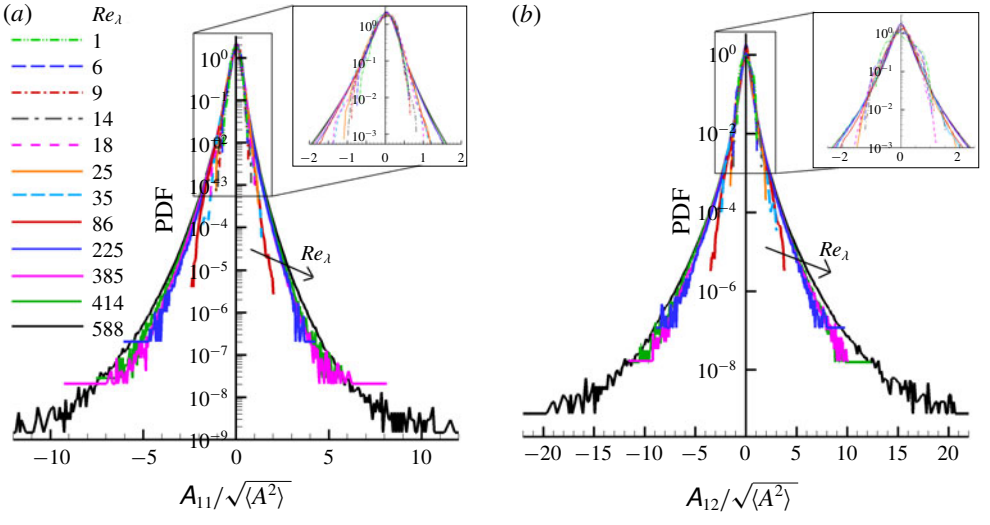

FIGURE 2. (Colour online) PDF of velocity-gradient component (*a*) $A_{11}/\sqrt{\langle A^2\rangle}$ (*b*) $A_{12}/\sqrt{\langle A^2\rangle}$ for different Re_λ.

The PDFs of A_{11} and A_{12} are shown in figure 2. As expected, at sufficiently high Re_λ, the longitudinal and transverse PDFs exhibit stretched exponential tails that grow with increasing Re_λ (Kailasnath, Sreenivasan & Stolovitzky 1992; Chevillard & Meneveau 2006; Schumacher *et al.* 2014).

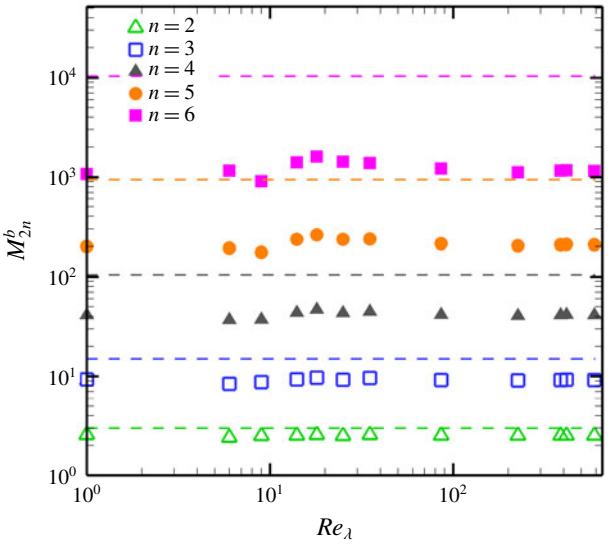

FIGURE 3. (Colour online) Even-order moments (M_{2n} for $n = 2, 3, 4, 5, 6$) of b_{11} as a function of Re_λ. Dashed lines represent Gaussian moments, i.e. $M^G_{2n} = (2n-1)!!$ for reference.

Another feature of turbulent flows relevant to this study is the dissipative anomaly (Donzis, Sreenivasan & Yeung 2005). In the asymptotic limit of high Re_λ, the normalized energy dissipation rate ($\epsilon L/u'^3$) asymptotes to a constant value of approximately 0.4–0.45. Here, L is the integral length scale and u' is the r.m.s. velocity. In other words, the normalized mean energy dissipation rate is independent of viscosity provided the value of Re_λ is sufficiently high. The onset of this dissipative anomaly in forced isotropic turbulence is observed at $Re_\lambda \sim 200$ (Sreenivasan 1998; Kaneda *et al.* 2003; Donzis *et al.* 2005). We will invoke this result later in the study.

4.2. *Normalized velocity-gradient statistics*

In this subsection, we investigate the statistical characteristics of the tensor $\boldsymbol{b}$. The even-order moments of b_{11} are given by

$$M^b_{2n} = \frac{\overline{{b_{11}}^{2n}}}{\overline{{b_{11}}^{2}}^{n}}. \tag{4.2}$$

Even-order moments (M^b_{2n} for $n = 2, 3, 4, 5, 6$) of b_{11} at different Re_λ are plotted in figure 3. b_{11}-moments are sub-Gaussian and nearly invariant across the entire Re_λ-range. This behaviour is to be expected as b_{ij} is bounded by unity. This also clearly demonstrates the contrast between the Reynolds number scaling of b_{ij} and A_{ij}.

We will next examine the PDFs of b_{ij} at different Re_λ. In figure 4(*a*,*c*) we present b_{11}- and b_{12}-PDFs, respectively, over the lower range of Reynolds numbers ($Re_\lambda \leqslant 35$). In this range, the PDF undergoes slight changes in shape with changing Re_λ. Figure 4(*b*,*d*) show that for $Re_\lambda \geqslant 35$, both b_{11}- and b_{12}-PDFs converge to a characteristic shape, which remains unchanged at higher Re_λ. This statistical self-similarity is anticipated from the collapse of higher-order moments of b_{11}

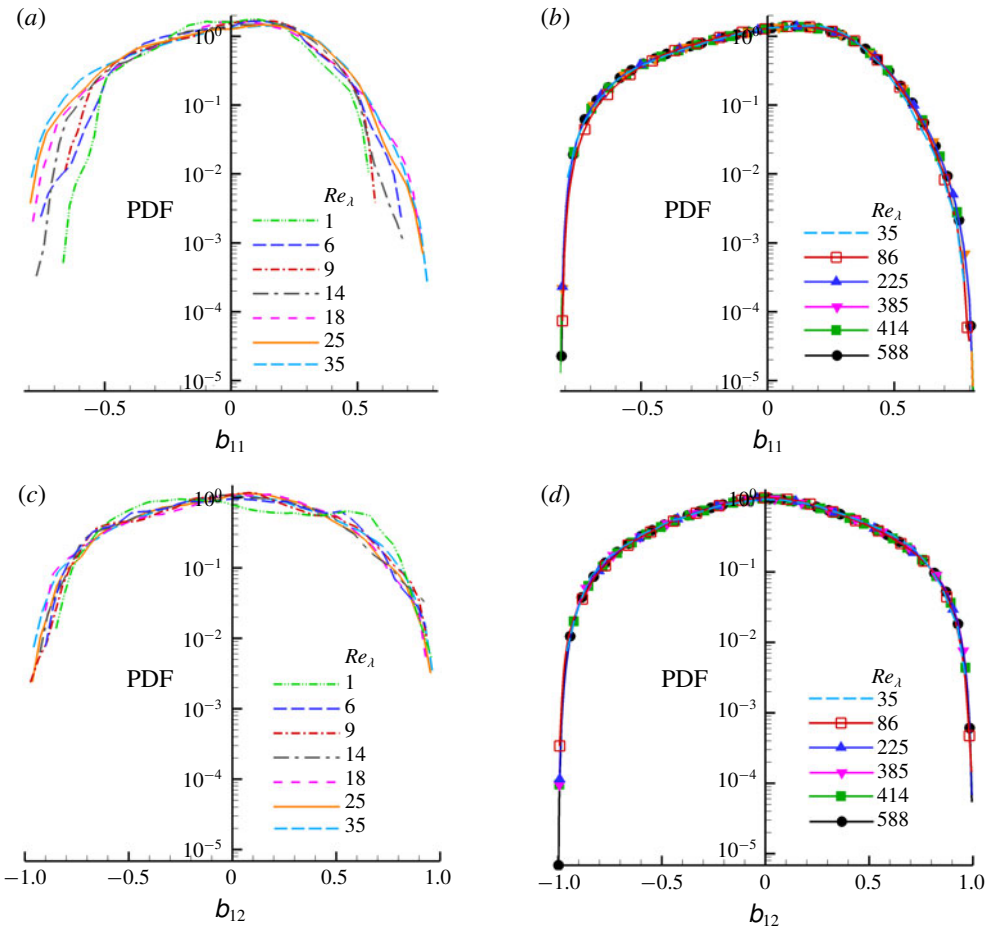

FIGURE 4. (Colour online) PDF of (*a*,*b*) normalized longitudinal velocity gradient b_{11} and (*c*,*d*) normalized transverse velocity gradient b_{12} for (*a*,*c*) $Re_\lambda = 1$–35 and (*b*,*d*) $Re_\lambda = 35$–588.

to constant values. Note that the minimum and maximum longitudinal (b_{11}) and transverse (b_{12}) velocity-gradient values are in accordance with the bounds obtained analytically in (2.12) and (2.13).

4.3. *Invariants of normalized velocity-gradient tensor*

Delving further, we examine the marginal PDFs of q and r in figures 5 and 6. Figure 5(*a*) shows that in the range where $Re_\lambda \leqslant 25$, the q-PDF appears to have a characteristic shape but shows discernible statistical variation about this shape. For $25 \leqslant Re_\lambda \leqslant 225$ (figure 5*b*), the distribution shifts towards more negative values of q with increasing Re_λ. In this range the probability of strain-dominated topology ($q < 0$) increases, while that of rotation-dominated topology ($q > 0$) decreases. This is due to the fact that viscosity affects the strain-dominated topologies more than rotation-dominated topologies and lower viscous influence at higher Reynolds numbers causes a higher percentage of strain-dominated topologies to be generated. Finally,

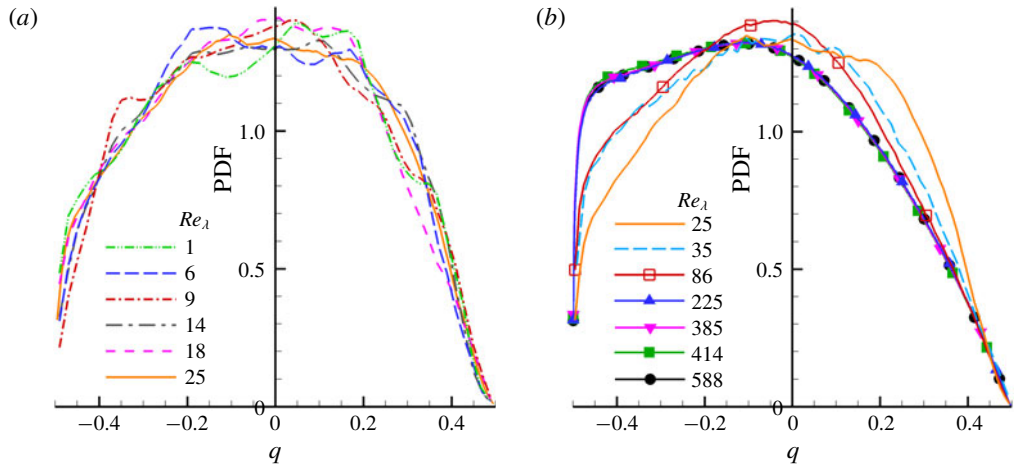

FIGURE 5. (Colour online) q-PDF for (*a*) $Re_\lambda = 1, 6, 9, 14, 18$ and 25 and for (*b*) $Re_\lambda = 25, 35, 86, 225, 385, 414$ and 588.

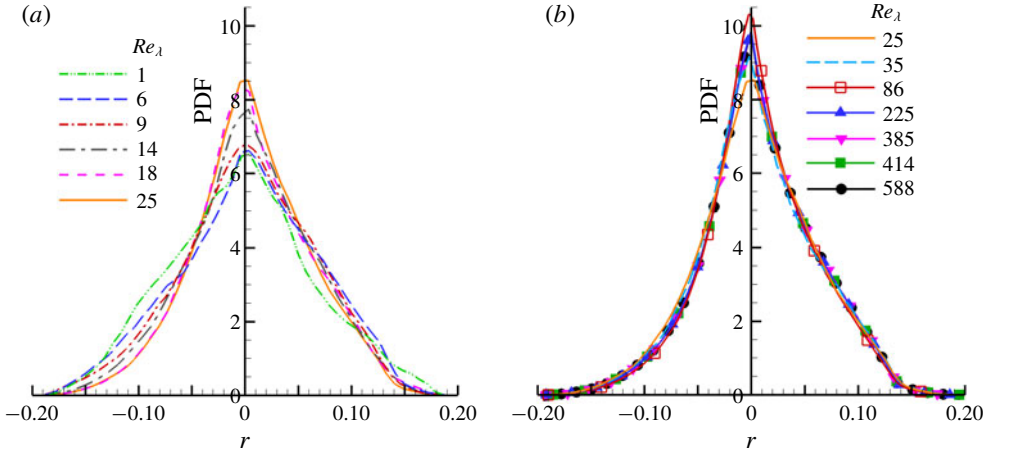

FIGURE 6. (Colour online) r-PDF for (*a*) $Re_\lambda = 1, 6, 9, 14, 18$ and 25 and for (*b*) $Re_\lambda = 25, 35, 86, 225, 385, 414$ and 588.

q-PDF attains a self-similar shape for flows above $Re_\lambda \sim 200$. In the middle range of $Re_\lambda \in (25, 200)$ the PDF transitions from one characteristic shape to another.

Unlike q-PDF, the r-PDF shows only a subtle Re_λ dependence. It may be noted from figure 6 that irrespective of the Re_λ value, r-PDF peaks at $r = 0$. The shape of r-PDF remains fairly unchanged while its peak increases with Re_λ in the range $Re_\lambda \in (1, 200)$. It appears to be invariant above $Re_\lambda \sim 200$. Note that the variation in r-PDF with Re_λ is minimal compared to q-PDF.

The q–r joint PDFs are plotted in figure 7 for different Re_λ. Figure 7(*a–f*) shows the variation in shape of the q–r joint PDF in the low-Re_λ range. At $Re_\lambda = 1$, the joint PDF is fairly symmetric about the q-axis and does not have a preferential distribution along the zero-discriminant (restricted Euler) line in the fourth quadrant. In fact, at this Re_λ the distribution resembles that of invariants of a Gaussian field (Pereira, Garban & Chevillard (2016)). As Re_λ increases in the range (1, 9), the q–r joint PDF

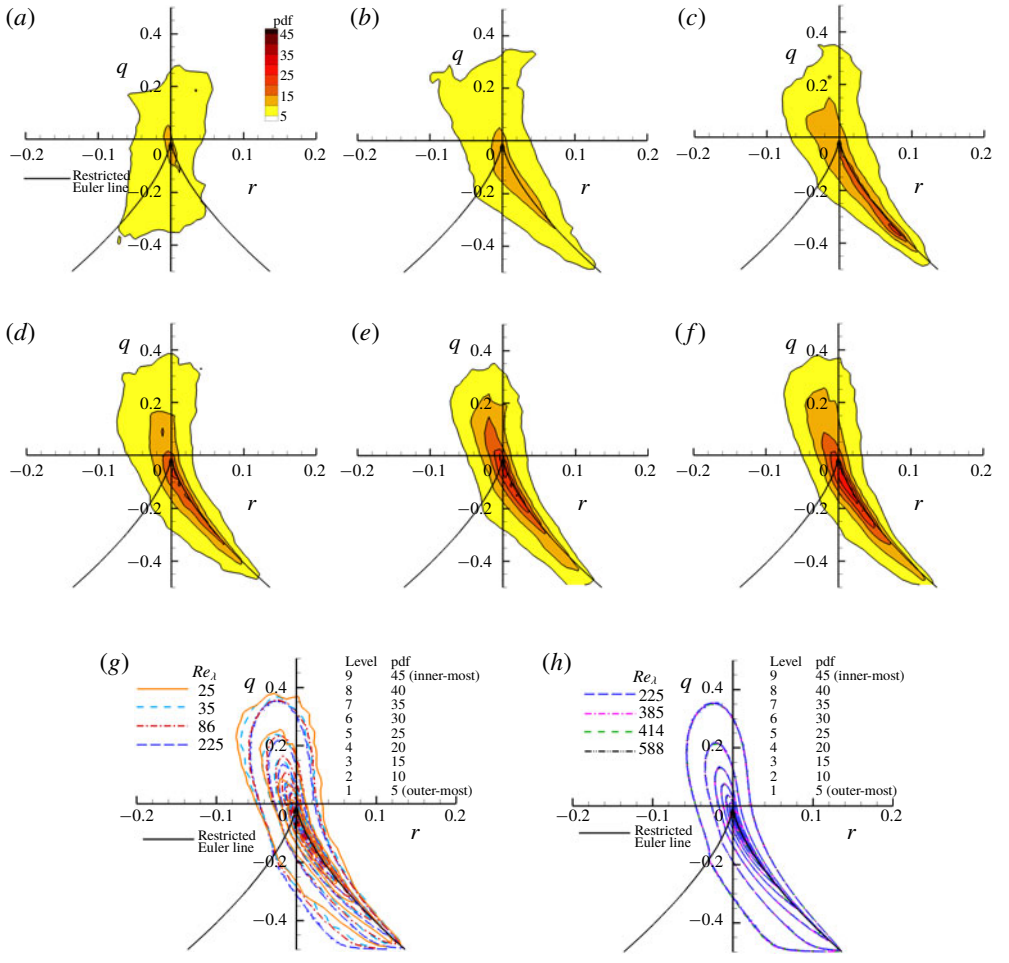

FIGURE 7. (Colour online) q–r joint PDF filled contour plots for Re_λ = (*a*) 1, (*b*) 6, (*c*) 9, (*d*) 14, (*e*) 18 and (*f*) 25. q–r joint PDF line contour plots for Re_λ = (*g*) 25 to 225 and (*h*) 225 to 588. The contour levels are identical for all plots: the colour scheme for (*a–f*) is shown in (*a*).

changes shape significantly and begins to develop a high-density region along the zero-discriminant line. It acquires a teardrop-like shape around $Re_\lambda = 9$. This value is in the same range as the transition Re_λ for onset of anomalous scaling of A_{ij} moments (Yakhot & Donzis (2017)). For $9 < Re_\lambda \leqslant 225$, the contours undergo refinements in the teardrop shape. Figure 7(*g*) clearly depicts these changes, amounting to an increase in the probability of strain-dominated topologies with respect to rotation-dominated topologies with increasing Re_λ. This reiterates the observation from the marginal PDF of q (figure 5). Finally, the joint PDF contours become invariant for $Re_\lambda > 200$, as shown in figure 7(*h*).

The joint q–r PDF exhibits three distinct ranges of variation with Re_λ. In the range $Re_\lambda \in (1, 10)$, it shows significant qualitative variation from near-Gaussian behaviour to a teardrop-like shape. Small quantitative changes are evident in the contours for $10 \leqslant Re_\lambda \leqslant 200$. Finally, an invariant joint distribution in the characteristic teardrop shape is attained for $Re_\lambda \geqslant 200$.

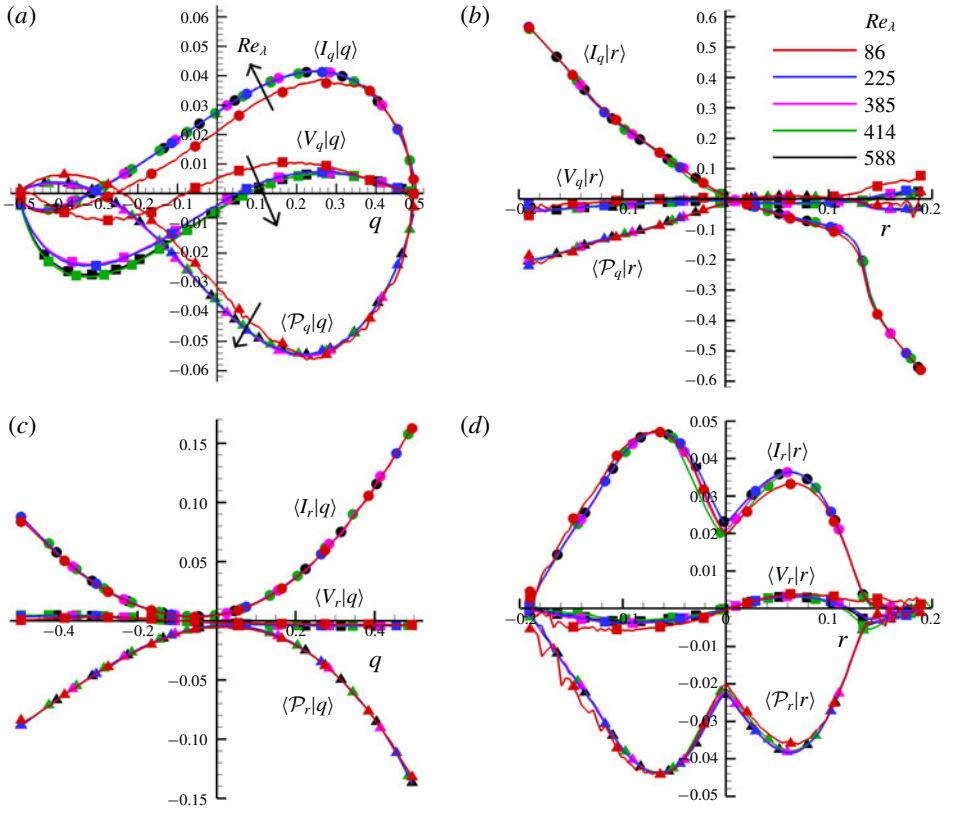

FIGURE 8. (Colour online) Conditional averages of inertial (circles), pressure (triangles) and viscous (squares) contributions in (*a*) $\langle \mathrm{d}q/\mathrm{d}t'|q\rangle$, (*b*) $\langle \mathrm{d}q/\mathrm{d}t'|r\rangle$, (*c*) $\langle \mathrm{d}r/\mathrm{d}t'|q\rangle$ and (*d*) $\langle \mathrm{d}r/\mathrm{d}t'|r\rangle$ for different Re_λ (refer to (2.23) and (2.27); colour scheme is given in (*b*)).

4.4. *Evolution of b_{ij}-invariants and A^2*

In this subsection we study the dynamics of q- and r-evolution which lays the foundation for modelling both b_{ij} and A^2. We also characterize the Re_λ dependence of θ-dynamics conditioned on q and r. We consider the Re_λ range 86–588 in this subsection to understand the role of different turbulent processes in q, r-phase space.

The averages of inertial, pressure and viscous terms of $\mathrm{d}q/\mathrm{d}t'$ (2.23) conditioned on q and r are plotted in figure 8(*a*,*b*). The inertial and pressure terms conditioned on q show a Re_λ dependence at low Re_λ and attain nearly invariant forms for $Re_\lambda \geqslant 225$. The viscous term conditioned on q shows a significant Re_λ dependence at low Re_λ values, but is nearly invariant in the higher range. All q-evolution terms conditioned on r appear to be completely insensitive to Re_λ.

The conditional averages of local (inertial and isotropic pressure), anisotropic pressure and viscous contributions in $\mathrm{d}r/\mathrm{d}t'$ (as shown in (2.27)) are reasonably insensitive to Re_λ, as shown in figure 8(*c*,*d*). The average viscous contributions (V_r) conditioned on both q and r are negligible in comparison to the other terms. This suggests that r-evolution is relatively impervious to viscosity and dominated by inertial and pressure terms. The fact that the probability distribution of r is nearly insensitive to Re_λ (figure 6*b*) is consistent with this inference.

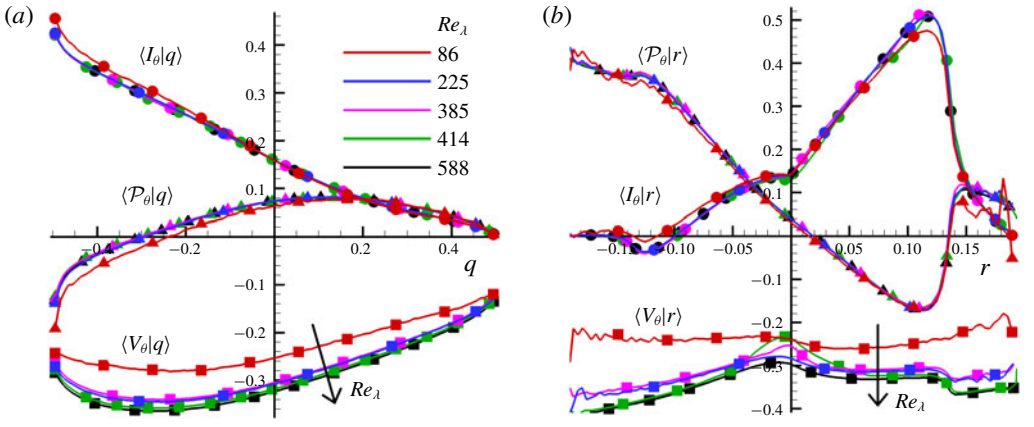

FIGURE 9. (Colour online) Conditional averages of inertial (circles), pressure (triangles) and viscous (squares) contributions in the θ-evolution equation conditioned on (*a*) q and (*b*) r for different Re_λ (refer to (2.17); colour scheme as given in *a*).

The different processes in the θ-evolution (as given in (2.17)) conditioned on q and r are plotted in figure 9(*a*,*b*). The average inertial term (I_θ) is positive for almost all q and r values – implying that inertia is a source of A^2. The sign of the pressure contribution ($\mathcal{P}_\theta$) depends on the q and r values. Expectedly, the viscous term (V_θ) is negative across all values of q and r, indicating that it is always a sink of A^2. Viscous effects are stronger in strain-dominated topologies ($q < 0$) and weaker in rotation-dominated topologies ($q > 0$). However, it is nearly independent of r. Overall, the conditionally averaged inertial and pressure processes in the θ-equation appear to approach asymptotic behaviour at high Re_λ (~ 200). The viscous term on the other hand appears to have a discernible Re_λ dependence throughout the Re_λ range.

Finally, we plot the conditional variance of the unclosed pressure and viscous terms in the q-, r- and θ-evolution equations in figure 10. The variance of the pressure term in q-evolution conditioned on both q and r have invariant forms irrespective of Re_λ (figure 10*a*,*c*). However, the conditional variance of the viscous contribution to $\mathrm{d}q/\mathrm{d}t'$ (figure 10*b*,*d*) does not converge even in the high-Re_λ limit. In fact, it shows a progressive increase in the magnitude of the variance with increasing Re_λ. Similarly, the conditional variance of the anisotropic pressure contribution in the r-evolution is invariant with changing Re_λ (figure 10*e*,*g*). On the other hand, the variance of the viscous term increases with increasing Re_λ (figure 10*f*,*h*). We also observe that the variance of $\mathcal{P}_\theta$ conditioned on both q and r exhibits reasonable collapse, while that of V_θ exhibits a distinct Re_λ dependence, with the magnitude increasing with Re_λ (figure 10*i*–*l*).

Therefore, we find that conditional statistics (mean and variance) of the pressure contribution to q-, r- and θ-evolution become nearly invariant for $Re_\lambda > 200$. The mean-viscous contribution to q- and r-evolution also exhibits self-similarity beyond $Re_\lambda > 200$. On the other hand, the conditional mean of the viscous term in θ-evolution shows a quantitative increase in magnitude with Re_λ. The conditional variance of pressure processes in q-, r- and θ-evolution are independent of Re_λ while that of the viscous contribution shows steady growth in magnitude with increasing Re_λ. This implies that the Re_λ dependence in the velocity-gradient dynamics is solely due to viscous effects, which is to be expected.

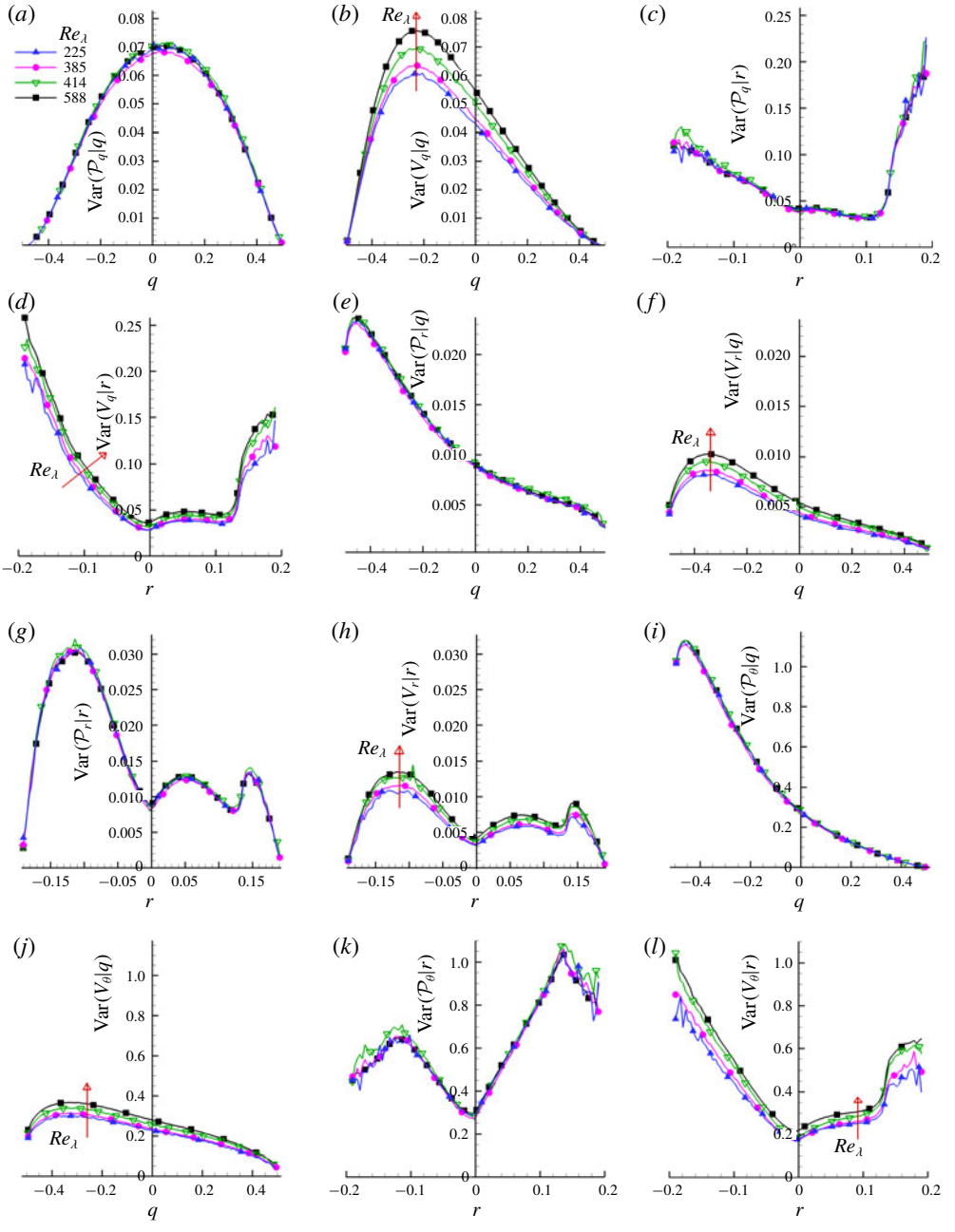

FIGURE 10. (Colour online) Conditional variance of pressure and viscous terms in the q-, r- and θ-equations conditioned on q and r: (*a*) $\mathrm{Var}(\mathcal{P}_q|q)$ versus q, (*b*) $\mathrm{Var}(V_q|q)$ versus q, (*c*) $\mathrm{Var}(\mathcal{P}_q|r)$ versus r, (*d*) $\mathrm{Var}(V_q|r)$ versus r, (*e*) $\mathrm{Var}(\mathcal{P}_r|q)$ versus q, (*f*) $\mathrm{Var}(V_r|q)$ versus q, (*g*) $\mathrm{Var}(\mathcal{P}_r|r)$ versus r, (*h*) $\mathrm{Var}(V_r|r)$ versus r, (*i*) $\mathrm{Var}(\mathcal{P}_\theta|q)$ versus q, (*j*) $\mathrm{Var}(V_\theta|q)$ versus q, (*k*) $\mathrm{Var}(\mathcal{P}_\theta|r)$ versus r and (*l*) $\mathrm{Var}(V_\theta|r)$ versus r for different Re_λ (colour scheme is given in *a*).

4.5. *Lagrangian velocity-gradient modelling*

One of the long-term goals of this work is to develop a Lagrangian stochastic model for velocity gradients along the lines of Girimaji & Pope (1990). The main distinction is that we plan to develop a model for b_{ij}-evolution rather than A_{ij}-evolution, as was the case in Girimaji & Pope (1990).

It is anticipated that h_{ij} and τ_{ij} will be more tractable than their A_{ij}-counterparts. The proposal is to decompose each term into a conditional mean and a stochastic (white noise) term:

$$h_{ij}(\boldsymbol{b}) = \langle h_{ij}|q, r, \boldsymbol{b}\rangle + h'_{ij}(q, r, \boldsymbol{b}), \tag{4.3}$$

$$\tau_{ij}(\boldsymbol{b}) = \langle \tau_{ij}|q, r, \boldsymbol{b}\rangle + \tau'_{ij}(q, r, \boldsymbol{b}). \tag{4.4}$$

The conditional statistics (means and variances) established in this paper (figures 8–10) provide guidance for this model development. Once h_{ij} and τ_{ij} models are established, Lagrangian evolution equations for A^2 and A_{ij} can be developed without the need for any further closures ((2.4) and (2.15)).

5. Summary and conclusions

The main objective of the work is to clearly characterize the Re_λ dependence of the different aspects of velocity-gradient structure and dynamics. In the analysis, we segregate the velocity-gradient magnitude (A^2) from the normalized-gradient tensor b_{ij}. The b_{ij}-tensor and the evolution of its invariants are the subject of this study. Some of the key findings of this study are summarized below:

(i) Higher-order moments (M^b_{2n}) of b_{ij} do not show any statistically significant variation across the entire range of Re_λ investigated in this study. This is in contrast with A_{ij}, which exhibits a significant increase of normalized moment values with increasing Re_λ. Moreover, A_{ij}-PDFs exhibit a clear stretch in tails as Re_λ increases, while b_{ij}-PDFs achieve self-similarity for $Re_\lambda > 35$.

(ii) PDFs and joint PDFs of b_{ij}-invariants (q, r) are more sensitive to changing Re_λ than individual b_{ij}-components:

  (*a*) The q–r joint PDF changes qualitatively for $Re_\lambda \in (1, 10)$ from Gaussian to a teardrop shape.

  (*b*) For $Re_\lambda \in (10, 200)$, the q–r joint PDF and marginal PDFs undergo minor quantitative changes with increasing Re_λ to accommodate an increasing proportion of strain-dominated topologies.

  (*c*) The q and r individual PDFs as well as the q–r joint PDF converge to the characteristic teardrop shape for $Re_\lambda > 200$. Note that this asymptotic behaviour is observed in a similar range of Re_λ as the onset of the dissipative anomaly (Donzis *et al.* 2005).

(iii) Physical processes contributing to the evolution of b_{ij}-invariants and A^2 are also examined:

  (*a*) For $Re_\lambda \geqslant 200$, the conditional mean and variance of the unclosed pressure term in the evolution of q, r and θ are independent of Re_λ.

  (*b*) The mean-viscous contribution to q- and r- evolution shows asymptotic convergence for $Re_\lambda > 200$. The mean-viscous contribution to θ-evolution does not vary qualitatively but shows a continued quantitative dependence on Re_λ. The conditional variance of viscous term in all three evolution equations continue to exhibit a Re_λ dependence.

(*c*) It is surmised that viscous processes are the primary source of the Re_λ dependence of A^2.

In future works, we plan to develop closure models for h_{ij} and τ_{ij} as a function of q and r. This will lead to a Lagrangian closure model for b_{ij}-evolution, and ultimately to A^2-evolution.

Acknowledgements

The authors would like to acknowledge Dr D. Donzis of Texas A&M University for providing the DNS data.

REFERENCES

ASHURST, W. T., KERSTEIN, A. R., KERR, R. M. & GIBSON, C. H. 1987 Alignment of vorticity and scalar gradient with strain rate in simulated Navier–Stokes turbulence. *Phys. Fluids* **30** (8), 2343–2353.

BECHLARS, P. & SANDBERG, R. D. 2017 Variation of enstrophy production and strain rotation relation in a turbulent boundary layer. *J. Fluid Mech.* **812**, 321–348.

BIKKANI, R. K. & GIRIMAJI, S. S. 2007 Role of pressure in nonlinear velocity gradient dynamics in turbulence. *Phys. Rev.* E **75** (3), 036307.

BLACKBURN, H. M., MANSOUR, N. N. & CANTWELL, B. J. 1996 Topology of fine-scale motions in turbulent channel flow. *J. Fluid Mech.* **310**, 269–292.

CANTWELL, B. J. 1992 Exact solution of a restricted Euler equation for the velocity gradient tensor. *Phys. Fluids* A **4** (4), 782–793.

CHEVILLARD, L. & MENEVEAU, C. 2006 Lagrangian dynamics and statistical geometric structure of turbulence. *Phys. Rev. Lett.* **97** (17), 174501.

CHEVILLARD, L., MENEVEAU, C., BIFERALE, L. & TOSCHI, F. 2008 Modeling the pressure Hessian and viscous Laplacian in turbulence: comparisons with direct numerical simulation and implications on velocity gradient dynamics. *Phys. Fluids* **20** (10), 101504.

CHONG, M. S., PERRY, A. E. & CANTWELL, B. J. 1990 A general classification of three-dimensional flow fields. *Phys. Fluids* A **2** (5), 765–777.

DANISH, M., SUMAN, S. & GIRIMAJI, S. S. 2016 Influence of flow topology and dilatation on scalar mixing in compressible turbulence. *J. Fluid Mech.* **793**, 633–655.

DONZIS, D. A., SREENIVASAN, K. R. & YEUNG, P. K. 2005 Scalar dissipation rate and dissipative anomaly in isotropic turbulence. *J. Fluid Mech.* **532**, 199–216.

DONZIS, D. A., YEUNG, P. K. & SREENIVASAN, K. R. 2008 Dissipation and enstrophy in isotropic turbulence: resolution effects and scaling in direct numerical simulations. *Phys. Fluids* **20** (4), 045108.

DONZIS, D. A. & SREENIVASAN, K. R. 2010 Short-term forecasts and scaling of intense events in turbulence. *J. Fluid Mech.* **647**, 13–26.

GIRIMAJI, S. S. & POPE, S. B. 1990 A diffusion model for velocity gradients in turbulence. *Phys. Fluids* A **2** (2), 242–256.

GIRIMAJI, S. S. & SPEZIALE, C. G. 1995 A modified restricted Euler equation for turbulent flows with mean velocity gradients. *Phys. Fluids* **7** (6), 1438–1446.

JEONG, E. & GIRIMAJI, S. S. 2003 Velocity-gradient dynamics in turbulence: effect of viscosity and forcing. *Theor. Comput. Fluid Dyn.* **16** (6), 421–432.

JOHNSON, P. L. & MENEVEAU, C. 2016 A closure for Lagrangian velocity gradient evolution in turbulence using recent-deformation mapping of initially Gaussian fields. *J. Fluid Mech.* **804**, 387–419.

KAILASNATH, P., SREENIVASAN, K. R. & STOLOVITZKY, G. 1992 Probability density of velocity increments in turbulent flows. *Phys. Rev. Lett.* **68** (18), 2766–2769.

KANEDA, Y., ISHIHARA, T., YOKOKAWA, M., ITAKURA, K. & UNO, A. 2003 Energy dissipation rate and energy spectrum in high resolution direct numerical simulations of turbulence in a periodic box. *Phys. Fluids* **15** (2), L21–L24.

LI, Y., PERLMAN, E., WAN, M., YANG, Y., MENEVEAU, C., BURNS, R., CHEN, S., SZALAY, A. & EYINK, G. 2008 A public turbulence database cluster and applications to study Lagrangian evolution of velocity increments in turbulence. *J. Turbul.* **9**, N31.

MARTÍN, J., DOPAZO, C. & VALIÑO, L. 1998*a* Dynamics of velocity gradient invariants in turbulence: restricted Euler and linear diffusion models. *Phys. Fluids* **10** (8), 2012–2025.

MARTÍN, J., OOI, A., CHONG, M. S. & SORIA, J. 1998*b* Dynamics of the velocity gradient tensor invariants in isotropic turbulence. *Phys. Fluids* **10** (9), 2336–2346.

MENEVEAU, C. 2011 Lagrangian dynamics and models of the velocity gradient tensor in turbulent flows. *Annu. Rev. Fluid Mech.* **43**, 219–245.

PEREIRA, R. M., GARBAN, C. & CHEVILLARD, L. 2016 A dissipative random velocity field for fully developed fluid turbulence. *J. Fluid Mech.* **794**, 369–408.

PEREIRA, R. M., MORICONI, L. & CHEVILLARD, L. 2018 A multifractal model for the velocity gradient dynamics in turbulent flows. *J. Fluid Mech.* **839**, 430–467.

SCHUMACHER, J., SCHEEL, J. D., KRASNOV, D., DONZIS, D. A., YAKHOT, V. & SREENIVASAN, K. R. 2014 Small-scale universality in fluid turbulence. *Proc. Natl Acad. Sci. USA* **111** (30), 10961–10965.

SORIA, J., SONDERGAARD, R., CANTWELL, B. J., CHONG, M. S. & PERRY, A. E. 1994 A study of the fine-scale motions of incompressible time-developing mixing layers. *Phys. Fluids* **6** (2), 871–884.

SREENIVASAN, K. R. 1998 An update on the energy dissipation rate in isotropic turbulence. *Phys. Fluids* **10** (2), 528–529.

SUMAN, S. & GIRIMAJI, S. S. 2010 Velocity gradient invariants and local flow-field topology in compressible turbulence. *J. Turbul.* **11** (2), N2.

VIEILLEFOSSE, P. 1982 Local interaction between vorticity and shear in a perfect incompressible fluid. *J. Phys.* **43** (6), 837–842.

WANG, X., SZALAY, A., ARAGÓN-CALVO, M. A., NEYRINCK, M. C. & EYINK, G. L. 2014 Kinematic morphology of large-scale structure: evolution from potential to rotational flow. *Astrophys. J.* **793** (1), 58.

YAKHOT, V. & DONZIS, D. 2017 Emergence of multiscaling in a random-force stirred fluid. *Phys. Rev. Lett.* **119** (4), 044501.

YAKHOT, V. & SREENIVASAN, K. R. 2005 Anomalous scaling of structure functions and dynamic constraints on turbulence simulations. *J. Stat. Phys.* **121** (5–6), 823–841.

YEUNG, P. K., ZHAI, X. M. & SREENIVASAN, K. R. 2015 Extreme events in computational turbulence. *Proc. Natl Acad. Sci. USA* **112** (41), 12633–12638.